Direct Observation on H-Elimination Enhancement from C_2H_4 through Non-Adiabatic Process by Femtosecond Laser Induced Coulomb Explosion

Wuwei Jin(金无维)[1,2], Chuncheng Wang(王春成)[1,2*], Xiaoge Zhao(赵晓戈)[1,2], Yizhang Yang(杨译章)[1,2], Dianxiang Ren(任殿相)[1,2], Zejin Liu(刘泽槿)[1,2], Xiaokai Li(李孝开)[1,2], Sizuo Luo(罗嗣佐)[1,2], and Dajun Ding(丁大军)[1,2*]

[1]*Institute of Atomic and Molecular Physics, Jilin University, Changchun 130012, China*
[2]*Jilin Provincial Key Laboratory of Applied Atomic and Molecular Spectroscopy, Jilin University, Changchun 130012, China*

(Received 28 February 2024; accepted manuscript online 16 April 2024)

Ethylene, the simplest model of a carbon-carbon double bond system, is pivotal in numerous chemical and biological processes. By employing intense infrared laser pump-probe techniques alongside coincidence measurements, we investigate the ultrafast non-adiabatic dynamics involved in the breakage of carbon-carbon double bonds and hydrogen elimination in dissociation of ethylene. Our study entails analyzing the dynamic kinetic energy release spectra to assess three bond-breaking scenarios, movements of nuclei, and structural changes around the carbon atoms. This allows us to evaluate the relaxation dynamics and characteristics of various dissociative states. Notably, we observe a significant rise in the yield of fragments resulting from C–H bond breakage with the delay time extended, suggesting non-adiabatic coupling through conical intersections from C–C bond breakage as a probable cause.

DOI: 10.1088/0256-307X/41/5/053101

Interactions of ultrafast, intense near-infrared laser pulses with molecules initiate a series of phenomena such as tunnel ionization, multiphoton ionization, dissociation, and Coulomb explosion (CE).[1–6] These processes are currently garnering interests for their intricate electron and nuclear dynamics. Employing sophisticated particle detection techniques to monitor progression of coherent nuclear wave packets, triggered by laser pulses and leading to bond disruption, deformation, or reconfiguration, is crucial for deepening our understanding of light-matter interactions and advancing control over chemical reactions.[7–11] There have been considerable investigations into the strong-field ionization of molecules, particularly in emitting vibrational wave packets of molecular cations, using pump-probe methodologies.[10,12,13] Studying nuclear motion following strong-field ionization not only sheds light on molecular dynamics at ultrafast scales but also facilitates the identification of transient structures and active potential energy surfaces (PESs), including conical intersections (CIs) and the roaming of intramolecular atoms or clusters.[14–16] Monitoring bond disruption during laser-induced Coulomb explosion imaging involves measuring the time-dependent kinetic energy release (KER) and fragment ion yields.[17–19] With picosecond to femtosecond temporal resolution, this technique enables the determination of molecular and cluster structures, thus allowing for real-time visualization of dynamic configurations of complex molecules and their dissociation processes.[20–22] Recent advances now permit ultrafast imaging of molecular or cluster bond lengths, geometric shapes, and conical intersections. Moreover, the intricate structural evolution of polyatomic molecules as they traverse the PES can be captured in real time.[15] Additionally, time-resolved structural evolution with angstrom-level spatial resolution on sub-femtosecond timescales has become feasible, providing comprehensive insights into the ionization and dissociation mechanisms of molecules in ultrafast laser fields.[23]

Photochemical reactions of the ethylene molecule (C_2H_4) and its cation have garnered considerable research interests due to the neutral molecule being the simplest model system with a carbon double bond, the cation as the most basic π radical system, and the most important organic chromophore involved in the photochemistry and photophysics of a majority of molecular systems. It is well-established that photoexcitation of both ethylene and its cation triggers ultrafast internal conversion processes and structural rearrangements, including twisting, pyramidalization, and isomerization, occurring within a femtosecond timeframe.[24–28] A majority of these studies have been focused on the extreme-ultraviolet (EUV) and x-ray ultraviolet (XUV) energy regions, where ultrafast relaxation dynamics of the ethylene cation have been observed in less than 50 fs. These processes predominantly involve decay from $\pi \rightarrow \pi^*$ excited states via conical intersections, transiting through Rydberg states to the ground state.[13,21,22,29–31] PESs are crucial in guiding the excited wave packet's evolution through non-adiabatic coupling

*Corresponding authors. Email: ccwang@jlu.edu.cn; dajund@jlu.edu.cn
© 2024 Chinese Physical Society and IOP Publishing Ltd

at these conical intersections.[32–34] Detailed discussions have been undertaken on the yield statistics of various dissociation channels and laser-controlled reaction pathways, with particular emphasis on the study of H-loss channels. Isotope techniques have been extensively utilized to monitor hydrogen dynamics at different molecular positions.[31,35–39] However, systematic studies on the temporal resolution and comparison of the nuclear dynamics evolution of multiple dissociation pathways are still lacking, particularly in relation to the carbon double bond's breakage, as well as the break of C–H bonds followed by subsequent H loss.

Prior studies have successfully distinguished and separated various electronic states in simple polyatomic molecules (ethane), under the influence of multi-orbital effects. This was achieved by analyzing photoelectron energy and momentum spectra during the ultrafast ionization dissociation processes, highlighting their distinct roles in subsequent reaction channels. Leveraging non-adiabatic coupling processes that facilitate state transitions, femtosecond time-resolved pump-probe techniques accompanied by delay time-dependent spectroscopic analyses have elucidated the timing and vibrational characteristics of electron-nuclear wave packets in the vicinity of conical intersections. These findings underscore the pivotal influence of non-adiabatic coupling dynamics on intramolecular hydrogen transfer mechanisms.[40] Our current research delves into the femtosecond dissociation dynamics of C_2H_4 cations, utilizing time-resolved Coulomb explosion imaging to capture the sequence of dissociation events triggered by strong-field ionization. Through the application of a delayed, intense laser pulse, we investigate varied dissociation routes of C_2H_4. Coincidence measurements serve to precisely delineate these pathways, unveiling evidence of potential non-adiabatic coupling dynamics among carbon-carbon and carbon-hydrogen bond breakage processes.

Experimental Method. The experimental setup integrates a pump-probe laser system with a cold target recoil ion momentum spectrometer (COLTRIMS).[41,42] Figure 1(a) illustrates the use of linearly polarized femtosecond laser pulses produced from a chirped pulse amplified Ti:sapphire system (40 fs, 800 nm, 1 kHz, 4 mJ) to investigate the ultrafast dissociation dynamics of ethylene molecules. For this work, we employ extended pulse widths to 200 fs for the reason that enhancement of some highly charged fragmental ions is formed with high kinetic energies.[35,43] Linearly polarized laser pulse (7.7×10^{14} W/cm^2) and elliptically polarized laser pulse (9.8×10^{14} W/cm^2, $\varepsilon = 0.77$) serve as the pump and probe laser beams, respectively. This choice enables clear disentanglement between ionization and dissociation processes. The polarization direction of the linearly pulse and the major axis of the elliptically pulse are aligned along the y axis, and the minor axis of the elliptically pulse is parallel to the z axis. These lasers, after passing through a Mach–Zehnder interferometer, are combined and focused within the COLTRIMS apparatus through a concave mirror ($f = 75$ mm). The pump laser induces ionization of ethylene molecules in a supersonic gas jet, producing a charged state. Subsequently, the probe laser further ionizes the molecules to even higher ionization states, causing Coulomb explosion and fragmentation into smaller ions. The time delay between the lasers is adjusted using a movable delay stage, with the zero time delay point identified by measuring the cross-correlation parent signal peak, exhibiting a cross-correlation profile with a full width at half maximum of approximately 80 fs. The ions generated are extracted in a homogeneous and weak electric field (14.5 V/cm) and then are directed onto a time and position-sensitive detector. This setup enables calculation of the ions' mass-to-charge ratio and three-dimensional momentum distribution. Further details about the experimental setup are available in our earlier publications.[2,44,45] Our scanning range for time delay spans from -2 ps to 6 ps, with each measurement step being 13.33 fs. Repeated scans reduce laser pulse jitter and accumulate ample data for robust analysis.

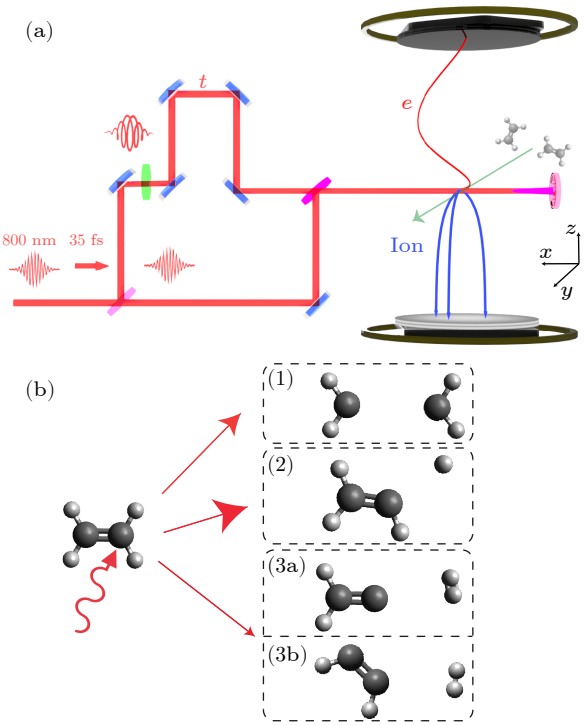

Fig. 1. (a) Schematic diagram of the experimental setup. A pump-probe setup with linearly and elliptically polarized laser pulses is built to track the ultrafast dissociation dynamics of molecules. (b) Sets of schematic diagrams that illustrate the molecular structures of Coulomb explosion channels involved in this study.

Results and Discussion. Figure 2 illustrates the time-resolved total KER spectra obtained from the CE channel shown in Fig. 1(b). We identify three distinct dissociation pathways in our study:

$$C_2H_4^{2+} \rightarrow CH_2^+ + CH_2^+, \quad (1)$$

$$C_2H_4^{2+} \rightarrow C_2H_3^+ + H^+, \quad (2)$$

$$C_2H_4^{2+} \rightarrow C_2H_2^+ + H_2^+. \quad (3)$$

Channel (1) is associated with the cleavage of the C–C double bond, channel (2) with the loss of a single hydrogen

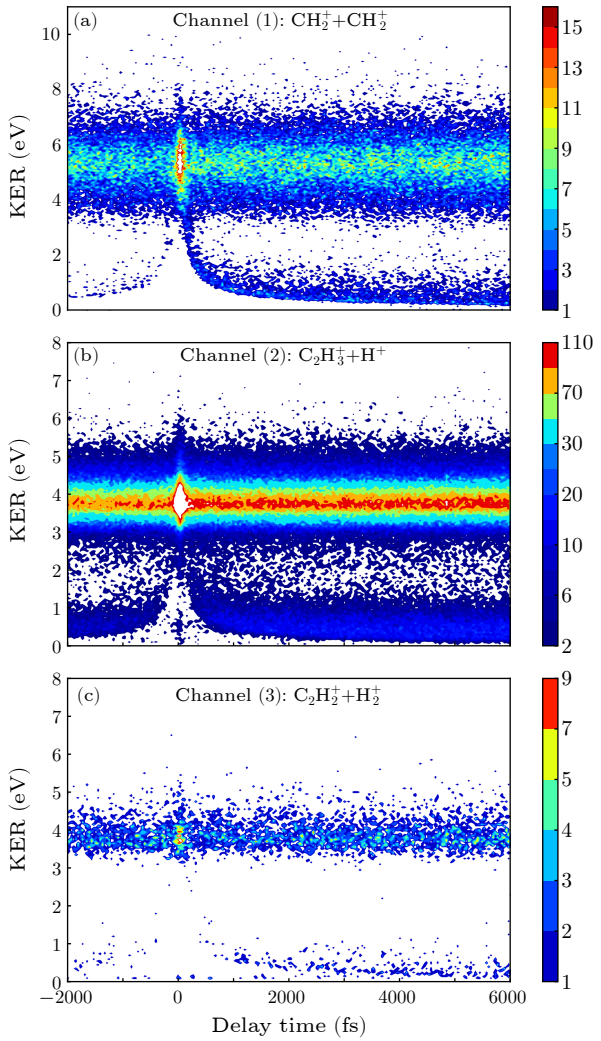

Fig. 2. (a)–(c) The measured time-dependent KER for the CE channels (1), (2) and (3). All CE pathways can be separated into direct CE and molecular bond breaking CE.

atom, and channel (3) with the formation of H_2^+. Given the molecular structure's symmetry, channel (3) should have two potential dissociation pathways: both hydrogen atoms originating from the same carbon atom or both hydrogen atoms coming from hydrogen atoms from different carbon atoms. In our study, we cannot distinguish these two pathways from each other. Previous isotope labeling methods have confirmed that these two pathways often coexist.[38] The latter scenario may involve twisted/pyramidalized and ethylidene configurations, with XUV/EUV excitation.[28,30,46] In our experiments, significant counts of CH_3^+ ions were not observed. Within the photo-ion and photo-ion coincidence (PIPICO) spectrum, no counts signal was found for mass-to-charge ratio (m/q) between 15 (CH_3^+) and 13 (CH^+). The extracted false coincidence data originated solely from channel (1), due to the m/q of CH_2^+ (14) being very close to that of the CH_3^+ (15) ion in PIPICO. However, a significant difference in slope allows for easy distinction between them. Meanwhile, previous literature regarding infrared (IR) laser pulse experiments does not mention any records of discovering the CH_3^+ channel, which is primarily reported within the XUV/EUV range. Each of these CE reactions occurs as a two-body process, resulting in splitting into two separate branches of fragments. For positive delay times, the pump laser first interacts with the molecule, leading to its ionization and dissociation, and then the probe laser examines the nuclear wavepacket along different ionic electronic states of the molecular cation. In contrast, negative delay suggests that the probe and pump roles are reversed. In Fig. 2(a), a notable peak at the zero-delay point arises from the cross correlation of the two laser beams. Importantly, at around 5.3 eV in KER, the count remains consistent regardless of delay time, which can be ascribed to the direct CE of $C_2H_4^{2+}$ solely induced by probe or pump pulses. In the other pathway, the KER gradually decreases over positive delay time, approaching asymptotic energy values. This delay time dependency indicates that these channels are induced by the combined contribution of the pump and probe laser pulses, embodying the temporal evolution information of the ethylene dissociation states. Figures 2(b) and 2(c) display similar characteristic profiles, primarily featuring two processes: direct CE and time-dependent molecular bond breaking CE. The KER for direct CE is identified to be around 3.7 eV, a value that results from the varying bond lengths and bond energies associated with the C–H bond. Additionally, the decay time associated with C–H bond breaking shows a distinct deviation from the patterns seen in C–C bond breaking.

The total KER from the time-resolved measurements is the cumulative result of the initial energy release (E_0) during the dissociation initiated by the pump laser and the Coulomb energy (E_{Coulb}) generated from the repulsion in two ions by the probe laser; thus, KER $= E_0 + E_{\text{Coulb}}$. Consequently, the Coulomb explosion process produces different asymptotic energies and time-dependent relationships across various dissociation pathways. Figure 3 illustrates the integrated KER spectra for all the three channels, normalizing the counts for comparison. The distinct peak at 5.3 eV for the C–C bond-breaking channel and the peaks at 3.7 eV for the hydrogen loss channels highlight their direct dissociation processes, which agrees well with the previous work.[35,36,47] The origins of these peaks correspond to states $^1B_{3u}$ [channel (1)] and ^3A_u (= T_1) [channels (2) and (3)]. Peaks observed below 2.8 eV are indicative of their respective bond-breaking dissociation events. Figure 4(a) showcases the KER peak positions for indirect dissociation pathways plotted against delay time for channels (1) and (2), mirroring the descending KER trajectory seen in Fig. 2 which underscored the evolving dynamics of the molecular structure. Each pathway has been fitted with an exponential curve, yielding decay times of 211±22 fs and 231±17 fs, respectively. Figure 4(b) displays the relationship between KER converted into corresponding internuclear distances over delay time, along with the same fitting curves. The corresponding asymptotic energies are 0.66 eV and 0.43 eV, respectively. These findings imply that the time evolution of dissociation for the two pathways, within a margin of error, exhibits no substan-

tial difference in time. The differences in the starting KER between channel (1) and channel (2) may reflect the differences of excited states involved in the evolution of different dissociation channels. Furthermore, channel (3) begins to show a significant increase in counts starting from approximately 400 fs. The peak height indicates that channel (3) has a higher relative ratio of dissociation through molecular bond breaking Coulomb Explosion rather than direct Coulomb Explosion, compared to channel (2) in Fig. 3.

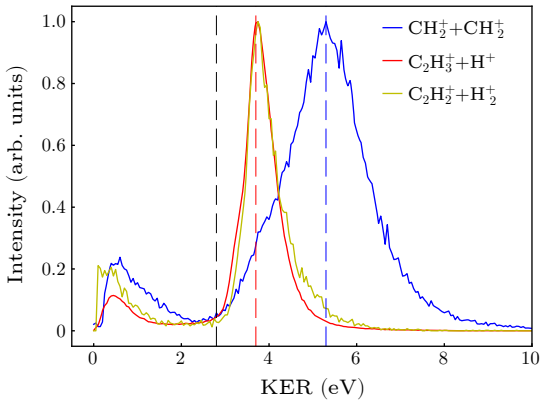

Fig. 3. KER spectra of the three channels from all pump-probe delay time. The black dashed line represents the position where the KER is 2.8 eV, which is also used to distinguish direct CE and molecular bond breaking CE. The red dashed line and the blue dashed line signify the peak positions at 3.7 eV and 5.3 eV, respectively, corresponding to their respective peak values.

To delve deeper into the electron-nucleus coupling dynamics during ethylene's dissociation, we continue to analyze the yield of time-dependent molecular bond-breaking CE channels across various delay times, normalizing the results for comparative analysis in Fig. 5, which reflect the dynamics on the PES. Figure 5(a) outlines the normalized counts for channels (1) and (2). Figure 5(b) displays the total counts for channel (3) due to low counting ratio at different delay times, complemented by their respective exponential fitting curves.

The function is given by

$$S_1(t) = \exp\left[\left(\frac{\sigma}{2\tau}\right)^2 - \frac{t}{\tau}\right] \cdot \left[1 - \mathrm{erf}\left(\frac{\sigma}{2\tau} - \frac{t}{\sigma}\right)\right], \quad (4)$$

$$S_2(t) = \left[1 - \exp\left(-\frac{t}{\tau_2}\right)\right], \quad (5)$$

where τ and τ_2 are decay/rise times, and σ is related to the full width at half maximum (FWHM) of the excitation pulse (170 fs).[48] Equation (5) provides the fitting curve for the rising part of the yield counts, while Eq. (5) describes the exponential decay process of the yields after rising to the steady stage ($t > 1000$ fs). According to the fitting outcomes, the rise time for the C–C bond-breaking channel (1) is 14 ± 1 fs, while it extends to 162 ± 60 fs for the hydrogen atom loss channel (2). C–H bond breakage requires approximately 162 fs of initiation time, in contrast to C–C bond dissociation, which necessitates virtually no initiation time. The rapid rate of C–C bond dissociation, relative to C–H bond breakage, underscores the influence of its distinct conical intersection and the configuration of its PES. Channel (2) needs to couple to different dissociative electronic states to undergo dissociation.

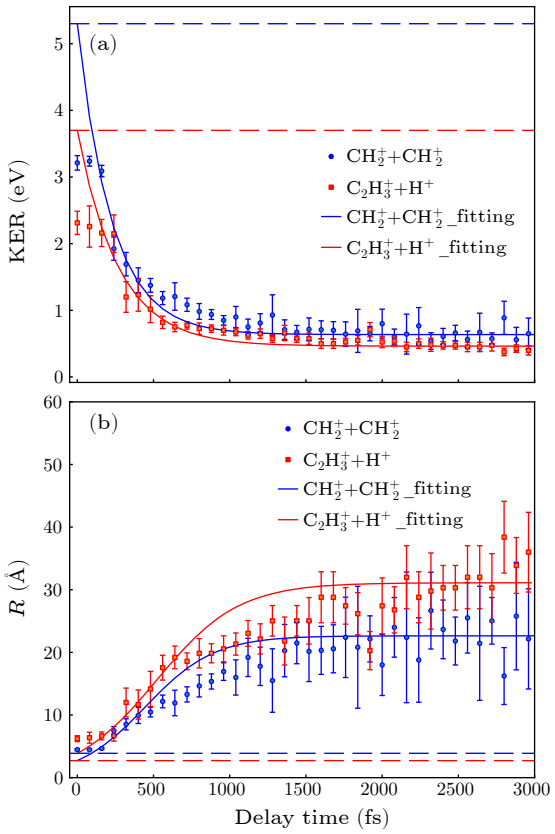

Fig. 4. (a) The KER corresponding to the peak counts at each delay time within the molecular bond breaking Coulomb explosion channels. The two CE channels are denoted by blue and red dots, respectively. The corresponding exponential fitting curves are represented by blue and red lines. The red and blue dashed lines indicate KER values of 3.7 eV and 5.3 eV, respectively. (b) Conversion of the KER into internuclear distance R as a function of delay time. This graph illustrates the trend of bond length variation as Coulomb explosion occurs for each channel. The red and blue dashed lines represent R values of 3.9 Å and 2.7 Å, respectively.

In the post-rise region, channel (2) exhibits a pronounced increase in signal as a function of delay time. In contrast, a more subtle declining trend is observed in channel (1). Subsequent examination of the counting ratio post-rise involves a second exponential fitting, as depicted in Eq. (5). Here, channel (1) demonstrates a slight decline, characterized by a decay time of 136 ± 75 fs. Conversely, channel (2) displays a marked increase, with a growth period of 1116 ± 896 fs. Upon reaching the asymptotic energy levels, the subsequent variations in yield for both channels are likely due to non-adiabatic coupling through conical intersections between the ground state and excited ionic states of ethylene. This coupling facilitates the transition of population between these two channels. This starting timescale of rising is also consistent with the results of previous studies (~ 1000 fs).[40] In Fig. 5(b), we cannot observe a significant rise curve in ion counts for channel (3), which is also reflected in Fig. 2(c). We infer that the for-

mation of this channel requires a longer time (> 400 fs) to manifest, involving the breakage of C–H bonds and the formation of HH bonds.

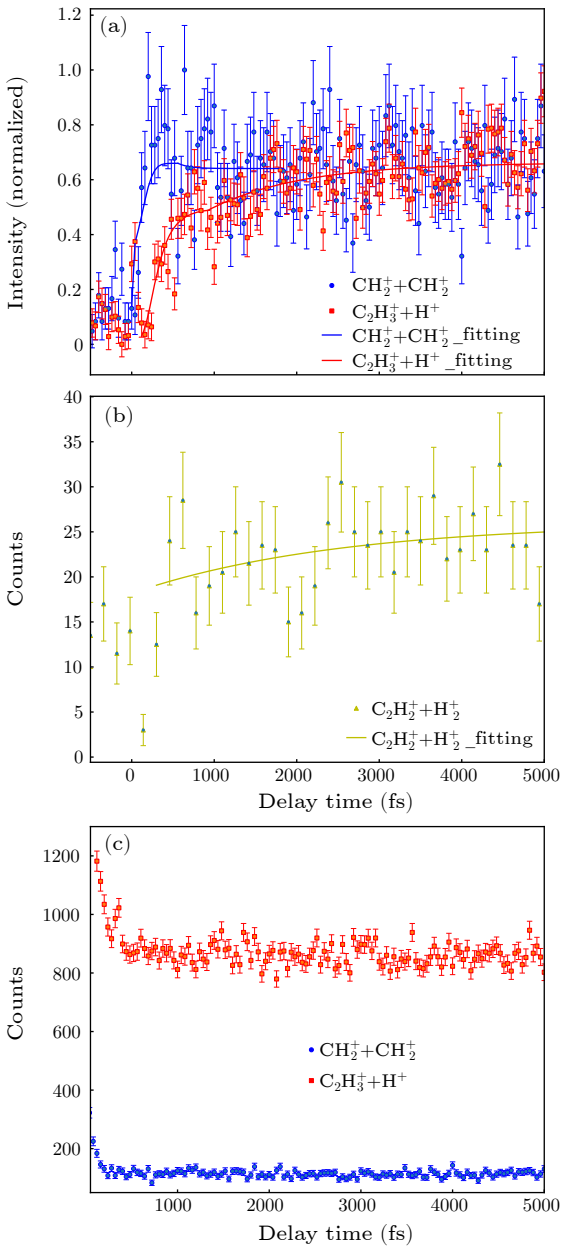

Fig. 5. (a) Normalized yields from the Coulomb explosion channel (1) and channel (2). Measured data and exponential fitting curves as a function of delay time are represented for each channel and their corresponding fitting curves in blue and red, respectively. (b) For Coulomb explosion channel (3), the counting yields, encompassing both the observed data and their exponential fits as they vary with delay time, are depicted in yellow. (c) The yield from the direct CE pathways of channels (1) and (2) as a function of delay time.

Subsequently, a similar signal growth was observed in channel (3) in the post-rise region, whereas channel (3) exhibits a clear growth with a rise time of 2500 ± 896 fs. A comparative analysis of the dissociation channel yield ratios over delay time after 1000 fs reveals that channel (2) contributes approximately 80%, followed by channel (1) at 18%, and channel (3) at 5%. Just after the delay time passes 0, the yield ratio for the C–C bond-breaking channel swiftly climbs to 40% due to fast C–C bond dissociation before diminishing to around 18% by 600 fs. To corroborate the observed increase in signal within channel (2) and the concurrent decrease in channel (3), we undertook a detailed analysis to extract and compare the yields of the direct CE counting ratio for these channels over delay times, aiming to discern any yield variation trends among different channels. Figure 5(c) demonstrates that the direct CE yields for both channels (1) and (2) remain relatively constant over time (> 500 fs), indirectly validating the delay time dependence observed along the molecular bond-breaking pathways. The noticeable enhancement in channel (2) is inferred to largely result from a diminishing contribution from channel (1). This observation suggests the potential involvement of non-adiabatic coupling dynamics in the observed phenomena.

In summary, we have performed pump-probe experiments utilizing femtosecond lasers to investigate the bond dissociation dynamics of ethylene. The time-resolved KER spectra of three distinct two-body dissociation channels are recorded. A significant delay of approximately 160 fs is noted in the dissociation timelines between the C–C and C–H bond breakage channels. We also conduct a detailed comparison of the highly similar yet subtly distinct dissociation pathways and asymptotic energy values between channels (2) and (3). We uncover a dynamic phenomenon wherein the yield of fragments from C–H bond breakage markedly increases over time, a behavior likely induced by non-adiabatic coupling through conical intersections. In contrast, a process with decreasing yield as a function of delay time has been detected for the C–C bond breakage channel. This observation suggests that the enhancement in H-elimination might be intricately linked with the C–C bond breakage process. To elucidate these dynamics further, comprehensive theoretical analyses and high-resolution experimental studies focusing on the escalation process, especially around near-zero delay times, will be instrumental in clarifying the coupling mechanisms involved.

Acknowledgment. This work was supported by the National Natural Science Foundation of China (Grant Nos. 12134005, 92261201, and 12274179).

References

[1] Sainadh U S, Xu H, Wang X, Atia-Tul-Noor A, Wallace W C, Douguet N, Bray A, Ivanov I, Bartschat K, Kheifets A, Sang R T, and Litvinyuk I V 2019 *Nature* **568** 75

[2] Luo S, Liu J, Li X, Zhang D, Yu X, Ren D, Li M, Yang Y, Wang Z, Ma P, Wang C, Zhao J, Zhao Z, and Ding D 2021 *Phys. Rev. Lett.* **126** 103202

[3] Hanus V, Kangaparambil S, Larimian S, Dorner-Kirchner M, Xie X, Schöffler M S, Paulus G G, Baltuška A, Staudte A, and Kitzler-Zeiler M 2019 *Phys. Rev. Lett.* **123** 263201

[4] Ji Q, Pan S, He P, Wang J, Lu P, Li H, Gong X, Lin K, Zhang W, Ma J, Li H, Duan C, Liu P, Bai Y, Li R, He F, and Wu J 2019 *Phys. Rev. Lett.* **123** 233202

[5] Li X, Yu X, Ma P, Zhao X, Wang C, Luo S, and Ding D 2022 *Chin. Phys. B* **31** 103304

[6] Yu X, Hu X, Zhou J, Zhang X, Zhao X, Jia S, Xue X, Ren D, Li X, Wu Y, Ren X, Luo S, and Ding D 2022 *Chin. Phys. Lett.* **39** 113301

[7] Ergler T, Rudenko A, Feuerstein B, Zrost K, Schröter C D, Moshammer R, and Ullrich J 2006 *Phys. Rev. Lett.* **97** 193001

[8] Bocharova I A, Alnaser A S, Thumm U, Niederhausen T, Ray D, Cocke C L, and Litvinyuk I V 2011 *Phys. Rev. A* **83** 013417

[9] Okino T, Furukawa Y, Nabekawa Y, Miyabe S, Amani Eilanlou A, Takahashi E J, Yamanouchi K, and Midorikawa K 2015 *Sci. Adv.* **1** e1500356

[10] Ibrahim H, Wales B, Beaulieu S *et al.* 2014 *Nat. Commun.* **5** 4422

[11] McDonnell M, LaForge A C, Reino-González J *et al.* 2020 *J. Phys. Chem. Lett.* **11** 6724

[12] Wei Z, Li J, Wang L, See S T, Jhon M H, Zhang Y, Shi F, Yang M, and Loh Z H 2017 *Nat. Commun.* **8** 735

[13] Zinchenko K S, Ardana-Lamas F, Seidu I, Neville S P, van der Veen J, Lanfaloni V U, Schuurman M S, and Wörner H J 2021 *Science* **371** 489

[14] Corrales M E, González-Vázquez J, de Nalda R, and Bañares L 2019 *J. Phys. Chem. Lett.* **10** 138

[15] Endo T, Neville S P, Wanie V, Beaulieu S, Qu C, Deschamps J, Lassonde P, Schmidt B E, Fujise H, Fushitani M, Hishikawa A, Houston P L, Bowman J M, Schuurman M S, Légaré F, and Ibrahim H 2020 *Science* **370** 1072

[16] Ekanayake N, Severt T, Nairat M, Weingartz N P, Farris B M, Kaderiya B, Feizollah P, Jochim B, Ziaee F, Borne K, Raju P K, Carnes K D, Rolles D, Rudenko A, Levine B G, Jackson J E, Ben-Itzhak I, and Dantus M 2018 *Nat. Commun.* **9** 5186

[17] Luo S, Zhou S, Hu W, Li X, Ma P, Yu J, Zhu R, Wang C, Liu F, Yan B, Liu A, Yang Y, Guo F, and Ding D 2017 *Phys. Rev. A* **96** 063415

[18] Zhao X, Yu X, Xu X, Yin Z, Yu J, Li X, Ma P, Zhang D, Wang C, Luo S, and Ding D 2020 *Phys. Rev. A* **101** 013416

[19] Zhao X, Xu T, Yu X, Ren D, Zhang X, Li X, Ma P, Wang C, Zhang D, Wang Q, Hu X, Luo S, Wu Y, Wang J, and Ding D 2021 *Phys. Rev. A* **103** 053103

[20] Kling N G, Díaz-Tendero S, Obaid R, Disla M R, Xiong H, Sundberg M, Khosravi S D, Davino M, Drach P, Carroll A M, Osipov T, Martín F, and Berrah N 2019 *Nat. Commun.* **10** 2813

[21] Ludwig A, Liberatore E, Herrmann J, Kasmi L, López-Tarifa P, Gallmann L, Rothlisberger U, Keller U, and Lucchini M 2016 *J. Phys. Chem. Lett.* **7** 1901

[22] Champenois E G, Shivaram N H, Wright T W, Yang C S, Belkacem A, and Cryan J P 2016 *J. Chem. Phys.* **144** 014303

[23] Zeller S, Kunitski M, Voigtsberger J *et al.* 2018 *Phys. Rev. Lett.* **121** 083002

[24] Köppel H, Domcke W, Cederbaum L S, and von Niessen W 1978 *J. Chem. Phys.* **69** 4252

[25] Lorquet J C, Sannen C, and Raseev G 1980 *J. Am. Chem. Soc.* **102** 7976

[26] Sannen C, Raşeev G, Galloy C, Fauville G, and Lorquet J C 1981 *J. Chem. Phys.* **74** 2402

[27] Farmanara P, Stert V, and Radloff W 1998 *Chem. Phys. Lett.* **288** 518

[28] Tao H, Allison T K, Wright T W, Stooke A M, Khurmi C, van Tilborg J, Liu Y, Falcone R W, Belkacem A, and Martinez T J 2011 *J. Chem. Phys.* **134** 244306

[29] Stert V, Lippert H, Ritze H H, and Radloff W 2004 *Chem. Phys. Lett.* **388** 144

[30] van Tilborg J, Allison T K, Wright T W, Hertlein M P, Falcone R W, Liu Y, Merdji H, and Belkacem A 2009 *J. Phys. B* **42** 081002

[31] Kosma K, Trushin S A, Fuss W, and Schmid W E 2008 *J. Phys. Chem. A* **112** 7514

[32] Martínez T J 2006 *Accounts Chem. Res.* **39** 119

[33] Joalland B, Mori T, Martínez T J, and Suits A G 2014 *J. Phys. Chem. Lett.* **5** 1467

[34] Kayi H, Garcia-Fernandez P, Bersuker I B, and Boggs J E 2013 *J. Phys. Chem. A* **117** 8671

[35] Xie X, Roither S, Schöffler M, Lötstedt E, Kartashov D, Zhang L, Paulus G G, Iwasaki A, Baltuška A, Yamanouchi K, and Kitzler M 2014 *Phys. Rev. X* **4** 021005

[36] Gaire B, Lee S Y, Haxton D J, Pelz P M, Bocharova I, Sturm F P, Gehrken N, Honig M, Pitzer M, Metz D, Kim H K, Schöffler M, Dörner R, Gassert H, Zeller S, Voigtsberger J, Cao W, Zohrabi M, Williams J, Gatton A, Reedy D, Nook C, Müller T, Landers A L, Cocke C L, Ben-Itzhak I, Jahnke T, Belkacem A, and Weber T 2014 *Phys. Rev. A* **89** 013403

[37] Gaire B, Haxton D J, Sturm F P, Williams J, Gatton A, Bocharova I, Gehrken N, Schöffler M, Gassert H, Zeller S, Voigtsberger J, Jahnke T, Zohrabi M, Reedy D, Nook C, Landers A L, Belkacem A, Cocke C L, Ben-Itzhak I, Dörner R, and Weber T 2015 *Phys. Rev. A* **92** 013408

[38] Stolow A, Balko B A, Cromwell E F, Zhang J, and Lee Y T 1992 *J. Photochem. Photobiol. A: Chem.* **62** 285

[39] Piancastelli M N, Stolte W C, Öhrwall G, Yu S W, Bull D, Lantz K, Schlachter A S, and Lindle D W 2002 *J. Chem. Phys.* **117** 8264

[40] Yang Y, Ren H, Zhang M, Zhou S, Mu X, Li X, Wang Z, Deng K, Li M, Ma P, Li Z, Hao X, Li W, Chen J, Wang C, and Ding D 2023 *Nat. Commun.* **14** 4951

[41] Dörner R, Mergel V, Jagutzki O, Spielberger L, Ullrich J, Moshammer R, and Schmidt-Böcking H 2000 *Phys. Rep.* **330** 95

[42] Ullrich J, Moshammer R, Dorn A, Dörner R, Schmidt L P H, and Schmidt-Böcking H 2003 *Rep. Prog. Phys.* **66** 1463

[43] Liang Q, Wu C, Wu Z, Liu M, Deng Y, and Gong Q 2009 *Chem. Phys.* **360** 13

[44] Wang C, Li X, Xiao X R, Yang Y, Luo S, Yu X, Xu X, Peng L Y, Gong Q, and Ding D 2019 *Phys. Rev. Lett.* **122** 013203

[45] Li X, Yu J, Xu H, Yu X, Yang Y, Wang Z, Ma P, Wang C, Guo F, Yang Y, Luo S, and Ding D 2019 *Phys. Rev. A* **100** 013415

[46] Lee S H, Lee Y T, and Yang X 2004 *J. Chem. Phys.* **120** 10983

[47] Ohrendorf E, Köppel H, Cederbaum L S, Tarantelli F, and Sgamellotti A 1989 *J. Chem. Phys.* **91** 1734

[48] Fiebig T, Chachisvilis M, Manger M, Zewail A H, Douhal A, Garcia-Ochoa I, and de La Hoz Ayuso A 1999 *J. Phys. Chem. A* **103** 7419